Editorial
Special Issue on Silicon–Germanium Alloys

I have enjoyed assembling this special issue of this journal on SiGe and I am grateful for the invitation to do so. In selecting the authors and topics I have tried to produce a timely and authoritive account of the current status of this important materials system. The first two papers are reviews on the material properties and device prospects of Si–Ge strained layer structures and a much needed overview of the bulk growth of SiGe. These are followed by two papers on the stability of strain and interfaces with thermal exposure. The genuinely exciting prospects for SiGe enhancing and extending silicon technologies have provided enormous motivation for researchers across the world. Much of their efforts have focused on actual devices notably the heterojunction bipolar transistor, and now that this device is well established, there is an increasing emphasis on field effect transistors. In addition the realisation of a silicon based optoelectronics technology would be a major prize there is intense activity in the investigation of the light emitting possibilities of two, one and zero dimensional Si–Ge structures. The remaining and major part of this issue deals with these aspects with an appropriate materials emphasis, as is apt for this journal.

Evan Parker
University of Warwick
September 1995

Numerical simulation of the temperature dependence of photoluminescence in strained-Si$_{1-x}$Ge$_x$/Si heterostructures

A. ST. AMOUR, J. C. STURM
Department of Electrical Engineering, Photonic and Opto-Electronic Materials Center (POEM), Princeton University, Princeton, NJ 08544 USA

In previous work it has been shown that the decay in photoluminescence from Si/strained-Si$_{1-x}$Ge$_x$/Si quantum wells at temperatures over 100 K is controlled by surface recombination and that the photoluminescence intensity can be increased by over an order of magnitude by surface passivation. These results had been explained only by a simple phenomenological model, which could not explain why at high pump power density the observed luminescence was constant from 77 to 250 K. This paper uses a two-carrier heterojunction device simulator to determine the carrier profiles during optical pumping. The profiles are used to understand quantitatively luminescence as a function of temperature and pump power density without making the over-simplifying assumptions required for analytical modeling. Surface recombination velocities over 10^3 cm/s drastically affect the results, and Auger recombination plays an important role at high pump power density.

1. Introduction

The demonstrated usefulness of strained-Si$_{1-x}$Ge$_x$ alloys on Si (1 0 0) in a variety of microelectronic device applications has motivated the study of the photoluminescence (PL) emitted from Si$_{1-x}$Ge$_x$/Si heterostructures. Most of the early work in this area was performed at very low temperatures (2–10 K) [1–3]. More recently, and motivated by the desire for a Si-based room temperature IR emitter [4, 5], there has been interest in the temperature dependence of the PL intensity [6–10]. We previously have reported clear evidence that the luminescence efficiency of high quality strained-Si$_{1-x}$Ge$_x$/Si heterostructures at high temperature is controlled by recombination at the top Si surface rather than by bulk Si$_{1-x}$Ge$_x$ or Si properties and that proper surface passivation can increase the room temperature Si$_{1-x}$Ge$_x$ PL by over an order of magnitude. Under some conditions we have observed Si$_{1-x}$Ge$_x$ luminescence which is essentially constant in intensity from cryogenic temperatures up to 250 K [10].

Some of these results were qualitatively explained by a phenomenological model, but the microscopic details were not well understood. In this paper, we use a numerical heterojunction device simulator to calculate the carrier densities throughout the Si$_{1-x}$Ge$_x$/Si heterostructure as a function of temperature and pump power. These results are then used to explain quantitatively the experimental luminescence characteristics without making the over-simplifying assumptions necessitated by an analytical model.

All experiments reported in this paper were performed on samples taken from a single wafer. The epitaxial Si and Si$_{1-x}$Ge$_x$ layers were grown by Rapid Thermal Chemical Vapor Deposition (RTCVD) on 100 mm Si (1 0 0) p-type ($\sim 10\,\Omega\cdot$cm) substrates. The Si$_{1-x}$Ge$_x$ layers were grown from dichlorosilane (DCS) and germane at 625 °C, while the Si was grown from DCS at 700 °C. Further details of our growth system and conditions are available elsewhere [11]. The as-grown structure consisted of a nominally undoped strained single Si$_{0.7}$Ge$_{0.3}$ quantum well (5 nm) on an undoped Si buffer (1.4 μm) and capped by approximately 25 nm of Si. The sample was oxidized at 800 °C for 10 minutes in a wet oxygen ambient resulting in about 10 nm SiO$_2$. It was then cleaved, and oxide was removed by dilute HF from part of the sample. In this way, the effect of the oxide could be experimentally separated from that of the thermal treatment received during oxidation.

2. Temperature dependence of PL intensity

The photoluminescence spectra of both pieces (with and without oxide cap) were measured from 6 to 300 K using a liquid nitrogen-cooled Ge detector and argon laser excitation at pump power densities of approximately 0.28 and 28 W/cm^2. Fig. 1 shows the evolution of the PL spectrum from the sample with oxide as a function of temperature. In the 6 K spectrum, the Si$_{1-x}$Ge$_x$ no-phonon (NP) line and the TO
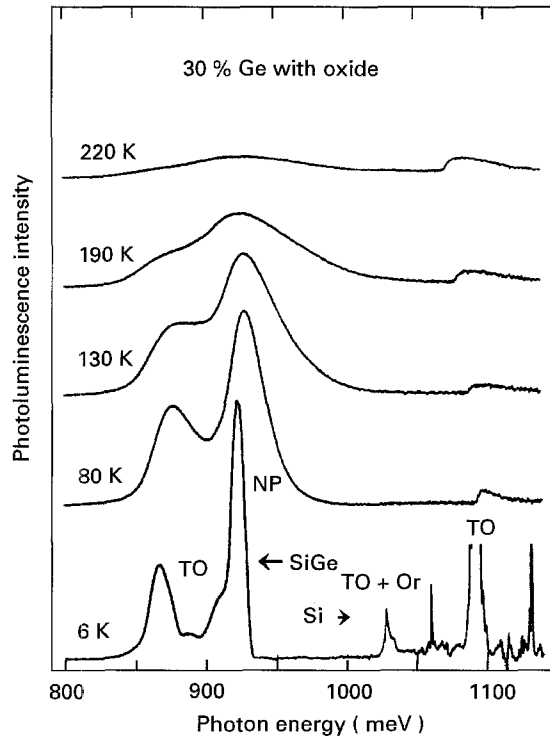
Figure 1 Photoluminescence spectra from the $Si_{0.7}Ge_{0.3}$ layer with an oxidized Si cap at five different temperatures. The pump power density was about 0.28 W/cm².

and TA phonon replicas were observed, while no sub-bandgap luminescence [12] was observed. This is evidence of high quality, uniform material. Note that in the 6 K spectrum, the Si TO replica has been cut off so as not to obscure the other spectra.

Plotted in Fig. 2 as a function of inverse temperature are the integrated $Si_{1-x}Ge_x$ PL intensities from the sample with oxide (at two pump power densities) and without oxide. The most striking feature of this data is the precipitous roll-off of the $Si_{1-x}Ge_x$ PL intensity at elevated temperatures. The data shows near constant intensity at low temperature and exponentially decaying intensity at high temperature. Inspection of the data reveals that the onset of the decay (the "knee" of the curve) is at higher temperature for the sample with oxide and even higher temperature for the high pump power density measurement. At room temperature, the PL intensity measured at high pump power density is down only by a factor of three from its low temperature value.

3. Analytical model

A qualitatively similar temperature dependence of PL from as-grown $Si_{1-x}Ge_x$ quantum wells with Si caps (i.e. sharply decreasing intensity at elevated temperature) has been observed by several other groups [6–8]. We have previously presented a simple model of this effect [9] in which we assumed no band bending, flat quasi-fermi levels, constant effective carrier lifetimes, Maxwell-Boltzmann statistics, and a radiative lifetime independent of temperature. The validity of these assumptions will be addressed later. This model yields a result for the measured integrated
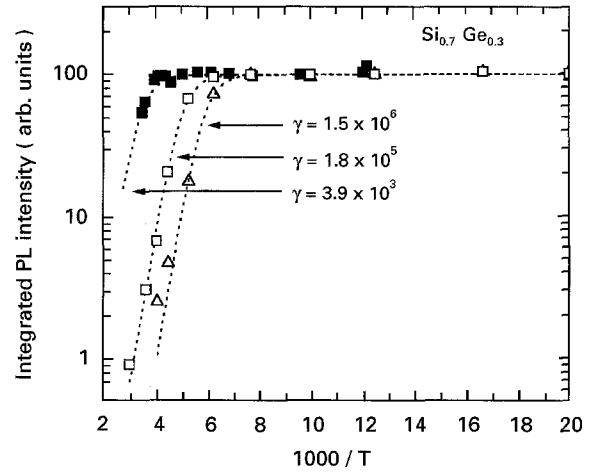

Figure 2 Integrated $Si_{1-x}Ge_x$ PL intensity as a function of inverse temperature. The data is fit to an analytical model. (△) without oxide, 0.28 W/cm², (□) with oxide, 0.28 W/cm², (■) with oxide, 28 W/cm², (- - -) model.

intensity of the $Si_{1-x}Ge_x$ luminescence, I_{SiGe}.

$$I_{SiGe} = \frac{C_1}{1 + \gamma e^{-\Delta E_g/kT}} \quad (1)$$

$$\gamma = \frac{\tau_{SiGe}W_{Si}}{\tau_{Si}W_{SiGe}} \quad (2)$$

τ_{SiGe} is the carrier lifetime in the $Si_{1-x}Ge_x$, and τ_{Si} is the effective lifetime in Si (including recombination at the top surface). ΔE_g is the band gap difference between Si and strained-$Si_{1-x}Ge_x$. W_{SiGe} is the width of the quantum well, and W_{Si} is the effective width of the Si in which the photogenerated carriers reside (on the order of the minority carrier diffusion length).

In the earlier paper [10], we fit the $Si_{1-x}Ge_x$ PL intensity data of Fig. 2 to Equation 1 using $\Delta E_g = 210$ meV (consistent with the change in bandgap of 230 meV relative to Si as measured by PL at 6 K). For the piece with its oxide stripped, $\gamma = 1.5 \times 10^6$; while for the piece with oxide remaining, $\gamma = 1.8 \times 10^5$. Of the factors in γ, only τ_{Si} could possibly have been changed by stripping the surface oxide, so we interpreted these results as changes in the effective lifetime in Si. Furthermore, given that the presence of oxide decreased γ by an order of magnitude, we have shown that τ_{Si} is determined by recombination at the top Si surface. Thus we concluded that the high temperature luminescence efficiency in high quality $Si_{1-x}Ge_x$ quantum wells is controlled by recombination at the top Si surface. That is, as the temperature increased, the $Si_{1-x}Ge_x$ PL intensity dropped off sharply even though a large fraction of the carriers were still confined to the quantum well because the total number of carriers in the entire sample decreased. If the recombination velocity of the top surface is sufficiently high, the few carriers in the Si cap will recombine very quickly (and pull more carriers out of the $Si_{1-x}Ge_x$). This leads to a large decrease in the average lifetime in the sample, and hence a diminished carrier density in the $Si_{1-x}Ge_x$ and reduced PL intensity.

The temperature dependence of the integrated $Si_{1-x}Ge_x$ PL intensity at high pump power density

was quantitatively very different from that at low pump power density. The low temperature behaviour was similar to that at low pump power density; the $Si_{1-x}Ge_x$ PL was constant as a function of temperature and was more than an order of magnitude stronger than the Si PL. The behaviour at high temperature (above 200 K), however, was strikingly different; the $Si_{1-x}Ge_x$ PL "knee" was pushed out to 250 K (see Fig. 2). The model was fit to the high pump power data for the sample with oxide with $\Delta E_v = 210$ meV as before, but with $\gamma = 3.9 \times 10^3$ (vs. 1.8×10^5 at low pump power density). Unfortunately, due to the many simplifying assumptions in the analytical model, it was not possible to use the model to understand this very interesting (and potentially useful) effect.

4. Numerical simulation of photoluminescence

Clearly understanding luminescence as a function of temperature requires accurate knowledge of the carrier distribution in the heterostructure. Accurate modeling of such distributions during optical pumping must take into account the heterostructure, potentially unequal lifetimes in different materials (and at interfaces), band bending due to charge accumulation in the quantum well or elsewhere, complications due to high carrier densities (such as Auger recombination and degeneracy), the diffusion of the photogenerated carriers, and so forth.

The analytical model described above neglected nearly all of these effects, and it was not possible to modify the model to include them. Therefore, we used a two-carrier heterojunction device simulator (Medici™ [13]) to solve for the carrier profiles as a function of temperature and optical pump power. The program does not include quantum confinement effects but does allow for the optical generation of carriers which decays exponentially as a function of depth.

The structure was simulated at temperatures between 100 and 300 K and with photogeneration rates of 5.3×10^{17} and 5.3×10^{19} cm^{-2} s^{-1}, corresponding to pump power densities of 0.28 and 28 W cm^{-2} assuming 2.4 eV photons (from an Ar$^+$ laser) and a surface reflectivity of 30%. The simulated absorption length was 1 μm. The model chosen in the simulator included both Shockley-Hall-Read (SHR) and Auger recombination.

$$R_{SRH} = \frac{pn - n_i^2}{TAUPO \cdot (n + n_i) + TAUNO \cdot (p + n_i)}$$

$$R_{Auger} = AUGN \cdot (pn^2 - nn_i^2)$$
$$+ AUGP \cdot (np^2 - pn_i^2) \qquad (3)$$

Table I lists the material parameters used in the simulation. For simplicity, we chose the density of states, mobilities, SHR lifetimes, and Auger recombination coefficients to be the same in Si and in $Si_{1-x}Ge_x$. A lower SHR lifetime in the $Si_{1-x}Ge_x$ relative to the Si would reduce the low temperature

TABLE I Parameters used by Medici™ in numerical simulation

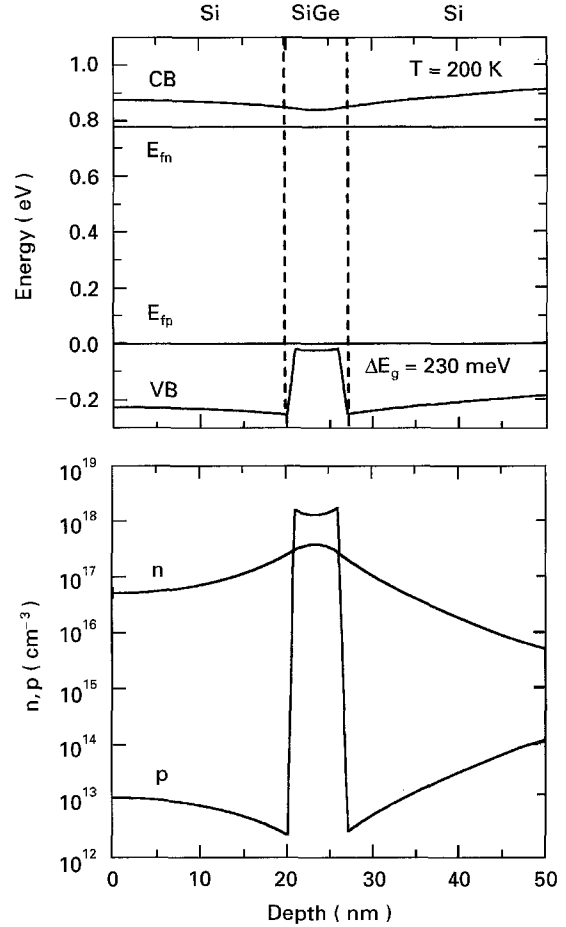| Constant SHR lifetime	Auger recomb. coefficients
TAUNO = 1 μs	AUGN = 2.8×10^{-31} cm^6/s
TAUPO = 1 μs	AUGP = 9.9×10^{-32} cm^6/s

Figure 3 Band diagram and carrier profiles of the near surface region for the structure simulated at 200 K. The pump power density was 0.28 W/cm^2 and $S_n = S_p = 0$. The dashed lines indicate the $Si_{1-x}Ge_x$/Si interfaces.

luminescence intensity and consequently raise the "knee" temperature. Also, in general, lower SHR lifetimes would partially mitigate the effects of surface recombination and Auger recombination. The effect of the top surface was included by selecting finite electron and hole recombination velocities. A germanium fraction of x = 0.35 was chosen to give $\Delta E_g = 230$ meV. The simulated structure was p-type with a uniform dopant density of 2×10^{16} cm^{-3}.

First we simulated the structure at various temperatures under low pump power density (0.28 W/cm). Fig. 3 shows the band diagram and carrier concentration profiles of the top 50 nm of our structure simulated at 200 K. Note that the fermi levels were flat indicating that the carrier profiles were determined by energetics, not kinetics. That is, the electron and hole populations in the $Si_{1-x}Ge_x$ were in equilibrium with their corresponding populations in the Si cap and in the top of the substrate. Also, we should note that there was considerable band bending, as can be more
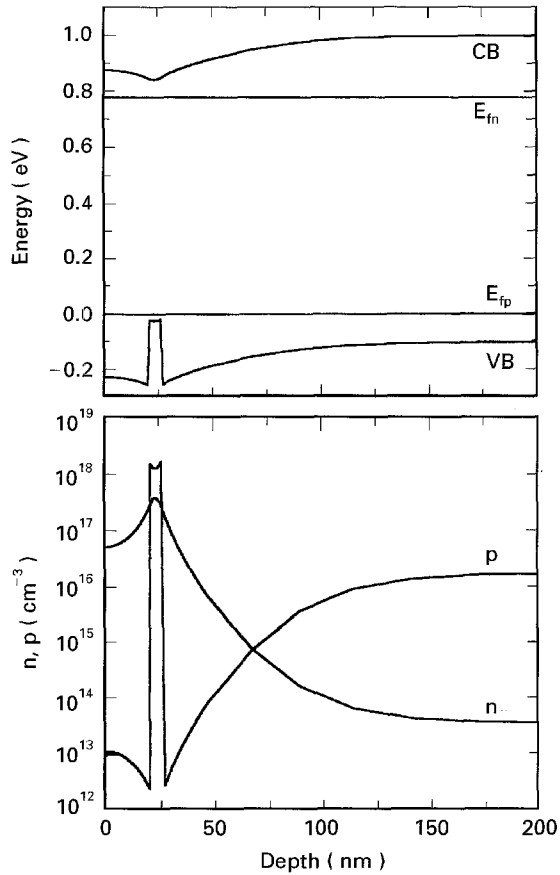
Figure 4 Band diagram and carrier profiles out to 200 nm for the same simulation as Fig. 3.

where B is the Einstein spontaneous emission coefficient and the integral is evaluated over the width of the $Si_{1-x}Ge_x$ layer.

In Si, exciton recombination is much more efficient than is band-to-band recombination. Even though in general only a small number of carriers form excitons, the PL in Si at low carrier densities up to 300 K is predominantly from excitons. The radiative efficiency of excitons is not a function of temperature, but the fraction of electrons and holes that form excitons is a strong function of n, p, and temperature with the result that B in general is a strong function of n, p, and temperature [14]. Presumably, these results apply equally to $Si_{1-x}Ge_x$ at low carrier densities. However, at carrier densities above the Mott transition, the luminescence is no longer from discreet excitons but rather is due to an electron-hole plasma (EHP) [15]. At these high carrier densities, the radiation is again proportional to the pn product because, through the phonon-assisted recombination process or the no-phonon recombination process in $Si_{1-x}Ge_x$ alloys, any conduction band electron can recombine equally well with any valence band hole. Furthermore, B should not be a strong function of temperature. We will later justify that the $Si_{1-x}Ge_x$ is indeed in this EHP regime even at low pump power density. So we will assume B to be independent of n, p, and temperature, with the result that the $Si_{1-x}Ge_x$ PL intensity is proportional to the pn product.

Fig. 5 shows simulation results for our structure. On this figure, we have simultaneously plotted the $Si_{1-x}Ge_x$ PL intensity data and the integrated pn product in the $Si_{1-x}Ge_x$. The PL data with and without oxide were independently renormalized so that their low temperature values over-laid the simulated curve. As mentioned previously, to simulate the difference between the sample with oxide and without,
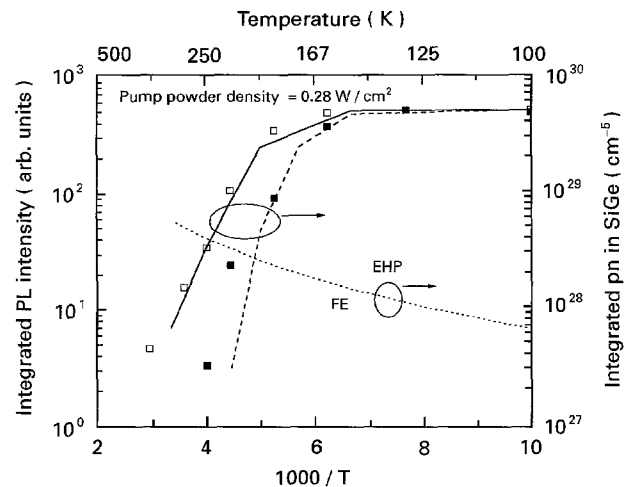
readily seen in Fig. 4 which displays the band diagram and carrier profiles out to 200 nm. Due to diffusion, the minority carrier (electron) concentration in the substrate exceeded its equilibrium value out to depths on the order of hundreds of microns. These last two observations (the significant band bending and the depth of the non-equilibrium carrier profile) already show that the assumption of no band bending of the earlier analytical model was not valid, demonstrating the usefulness of the full two-carrier numerical simulation approach.

The bandgap difference between Si and strained-$Si_{1-x}Ge_x$ is contributed predominantly by the valence band. In fact, Medici™ takes $\Delta E_v = \Delta E_g$ and $\Delta E_c = 0$. Consequently, the quantum well efficiently captured holes, leading to the band bending. The coulomb potential of these positive charges attracted electrons resulting in an electron distribution with a clear peak at the center of the well, which in most cases was nearly equal to the hole density. In the Si regions adjacent to the $Si_{1-x}Ge_x$ well, the electron density greatly exceeded the hole density; but deeper into the substrate (> 100 nm), electrons became the minority carrier because of the uniform p-type doping.

To compare device simulation results to PL intensity data it is necessary to make some assumptions about the relationship between photon generation and the electron and hole densities. In general, one can write that the PL intensity I_{SiGe} is given by

$$I_{SiGe} = \int B \cdot np.dx \qquad (4)$$

Figure 5 Comparison of the measured integrated $Si_{1-x}Ge_x$ PL intensity data to the simulated integrated pn product in the $Si_{1-x}Ge_x$ as a function of temperature for low pump power. The carrier density for the Mott transition between free excitons (FE) and an electron-hole plasma (EHP) is also indicated. The PL data was vertically scaled to overlay the simulation at low temperature. S_n and S_p are the electron and hole surface recombination velocities. (□) with oxide, (■) without oxide, (—) $S_n = S_p < 10^3$ cm/s (- - -) $S_n = S_p < 10^5$ cm/s (- - -) Mott criteria.

we varied the recombination velocities (S_n and S_p) of the top Si surface. Small amounts of fixed charge as is normally found at oxide/Si interfaces (up to 10^{11} cm^{-2}) were found to have little effect on the results, probably because the high carrier concentrations in the near surface region drown out the effect of reasonable fixed charge densities. Therefore, results presented are all for no fixed charge.

In confirmation of our previous work, we have shown that a surface recombination velocity on the order of 10^5 cm/s is required to fit the data from the sample without oxide, while the data from the sample whose top surface is passivated with oxide can be fit with velocities less than 10^3 cm/s. In addition, similar to the earlier model, both sets of simulations show a high temperature decay activation energy approximately equal to ΔE_g. Also shown is the line for the Mott transition from free excitons (FE) to an electron-hole plasma ($n_{crit} = k_B T / 16 \pi E_x a_x^3$) [16]. Note that, except for some points well above the "knee" temperature, our assumption of an EHP in the Si$_{1-x}$Ge$_x$ and constant B is justifiable.

Next, we turned to the pump power dependence, which could not be explained with our simple analytical model. We re-simulated our heterostructure changing only the pump power density. In Fig. 6, we have replotted the low pump power data and simulation results along with the high power data and simulation results. Again, the PL data points were independently renormalized to match the simulated points. Close inspection of the simulated sets of points reveals that increased pump power not only raises the pn product but also pushes the "knee" out to higher temperature as in the PL data. The "knee" of the low pump power density data and simulation is at 200 K, while that of the high pump power data is at 265 K. The high pump power simulation accounts for about half of this shift, and reasonable parameter adjustment could account for the rest (see Fig. 6, dashed curve).

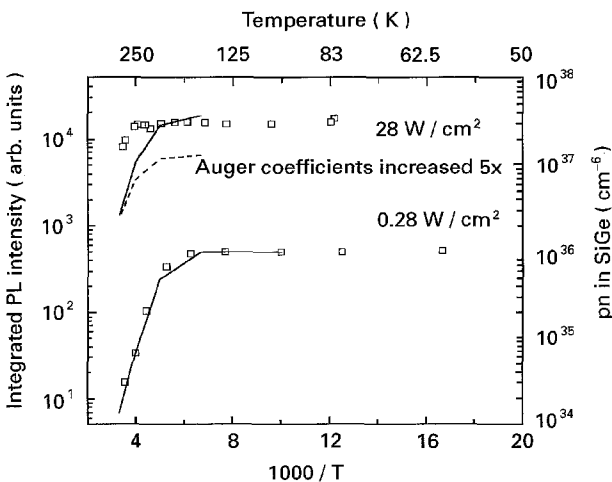The root cause of this behaviour (increasing "knee" temperature with increasing pump power density)

is Auger recombination in the Si$_{1-x}$Ge$_x$ which lowers the lifetime of carriers when the concentrations are high, as they are at high pump power and low temperature. In this regime, the electron and hole concentrations in the Si$_{1-x}$Ge$_x$ layer approach 10^{19} cm^{-3}, reducing the free carrier lifetime. For example, at low pump power density, the simulated effective lifetime ($\tau \equiv n'/R$) in the centre of the Si$_{1-x}$Ge$_x$ layer is 0.81 μs at 150 K. However, at two orders of magnitude higher pump power density, the effective lifetime is only 0.065 μs, showing the strength of the Auger effect. Also note the pn product (and consequently the PL intensity) is up only thirty times despite a 100 times increase in pump power density.

As the temperature is raised, electrons and holes are thermally excited from the quantum well, lowering their density, slowing the rate of Auger recombination, and thus raising the effective lifetime. This results in a net increase in the total number of free carriers in the sample (Si and Si$_{1-x}$Ge$_x$). Even though the fraction of carriers in the Si$_{1-x}$Ge$_x$ well decreases sharply with increasing temperature, the total number of electrons and holes confined to the well remains nearly constant. This is demonstrated in Fig. 7, where we have plotted the pn products in Si$_{1-x}$Ge$_x$ and the average lifetime τ_{ave} as a function of inverse temperature. The average lifetime is defined as

$$\tau_{ave} = \frac{1}{P_{total}} \int n' \cdot dx \qquad (4)$$

where P_{total} is the total photogeneration rate and n' is the total excess electron density throughout the entire sample induced by the optical pumping. At low pump power, τ_{ave} is nearly independent of temperature and near the SHR recombination lifetime of 1 μs. In contrast, at high pump power density, τ_{ave} is less than 0.1 μs at 150 K but increases exponentially with inverse temperature. This is because at low pump power density Auger recombination is not significant; while at high pump power, it is dominant at low temperature (very high carrier concentrations in the quantum
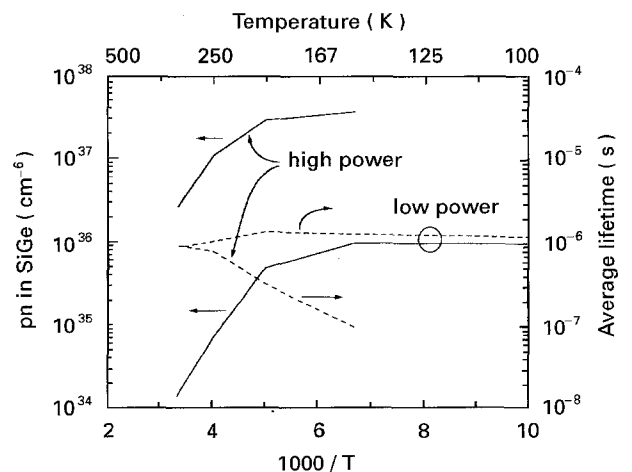

Figure 6 Comparison of the low and high pump power density results. The left axis is the measured integrated Si$_{1-x}$Ge$_x$ PL intensity data. The right axis is the simulated pn product at the center of the Si$_{1-x}$Ge$_x$ layer. The PL data was vertically scaled to overlay the simulation at low temperature.

Figure 7 Comparison of the low and high pump power density simulation results. The left axis is the simulated pn product at the center of the Si$_{1-x}$Ge$_x$ layer. The right axis is the average lifetime in the entire sample, $\tau_{ave} = 1/P_{total} \int n' \cdot dx$. P_{total} is the total photogeneration rate.

well) and becomes less significant at the temperature is raised.

In principle, other mechanisms besides Auger recombination might be able to explain the difference in PL intensity verses temperature for high and low pump power. According to the earlier analytical model, the "knee" position is determined by three factors which could be influenced by pump power density: (1) ΔE_g, (2) τ_{Si}, and (3) τ_{SiGe}. High carrier concentrations (as would be present at high pump power density) are known to reduce the bandgap in both Si and $Si_{1-x}Ge_x$. For this effect to be the sole explanation for our data, 100 meV of bandgap narrowing in the $Si_{1-x}Ge_x$ at high pump power with respect to low pump power would be required. The contributions to bandgap narrowing can be divided into two classes: (1) those involving carrier-impurity interactions and (2) those involving carrier-carrier interactions. Because our material was nominally undoped, the first class should be neglected. Using only the exchange and correlation expressions of Jain and Roulston [17] and carrier densities from simulations (with Auger recombination set to zero), we found the bandgap narrowing shift to be less than a quarter of that required to fit the data.

An increase in the effective lifetime in Si τ_{Si} also would have the effect of increasing the "knee" temperature. To fit our data, an increase of the effective lifetime in Si of 50X would be required. Through our simulations, we have shown that for well passivated surfaces the recombination velocities are small ($< 10^3$ cm/s) and surface recombination ceases to play the determining role, so that the increase would have to be due to bulk effects. High-level injection has the potential for significantly increasing the excess carrier lifetime in bulk Si in cases where the minority carrier density nearly equals the majority carrier density. However, this condition exists only within the top 100 nm of our samples (see Fig. 4), while τ_{Si} is determined primarily by the electrons deep in the substrate (if the top surface is passivated). Consequently, high-level injection is not a likely explanation of our data. Therefore, we conclude that the difference in the temperature dependence of the PL intensity at high and low pump power density is due to Auger recombination in the $Si_{1-x}Ge_x$, and not to bandgap narrowing in the $Si_{1-x}Ge_x$ or high-level injection in the Si.

5. Conclusions

We have employed a two-carrier heterojunction device simulator to investigate the temperature and pump power density dependence of the photoluminescence intensity from a strained-$Si_{1-x}Ge_x$ quantum well. The numerical simulation accurately modeled the experimental results that the PL intensity at high temperature depends of the passivation of the top Si surface and that the activation energy of the high

temperature decay approximately equals ΔE_g. The numerical simulator gives quantitative information on carrier profiles throughout the sample, something not possible with analytical models. Finally, the simulation results enabled us to explain the mechanism responsible for the experimental observation that PL intensity can be constant up to 250 K at high pump power density.

References

1. K. TERASHIMA, M. TAJIMA and T. TATSUMI, *Appl. Phys. Lett.* **57** (1990) 1925.
2. J. C. STURM, H. MANOHARAN, L. C. LENCHYSHYN, M. L. W. THEWALT, N. L. ROWELL, J. -P. NOEL and D. C. HOUGHTON, *Phys. Rev. Lett.* **66** (1991) 1362.
3. D. DUTARTE, G. BREMOND, A. SOUIFI and T. BENYATTOU, *Phys. Rev. B* **44** (1991) 11525.
4. D. J. ROBBINS, P. CALCOTT and W. Y. LEONG, *Appl. Phys. Lett.* **59** (1991) 1350.
5. Q. MI, X, XIAO, J. C. STURM, L. C. LENCHYSHYN and M. L. W. THEWALT, *ibid.* **60** (1992) 3177.
6. S. FUKATSU, N. USAMI and Y. SHIRAKI, *Jpn. J. Appl. Phys.* **32** (1993) 1502.
7. M. WACHTER, F. SCHÄFFLER, H.-J. HERZOG, K. THONKE and R. SAUER, *Appl. Phys. Lett.* **63** (1993) 376.
8. M. GAIL, J. BRUNNER, U. MENCZIGAR, A. ZRENNER and G. ABSTREITER, *Mat. Res. Soc. Symp. Pro.* **298** (1993) 21.
9. J. C. STURM, A. ST. AMOUR, Q. MI, L. C. LENCHYSHYN and M. L. W. THEWALT, *Jpn. J. Appl. Phys.* **33** (1994) 2329.
10. A. ST. AMOUR, J. C. STURM, Y. LACROIX and M. L. W. THEWALT, *Appl. Phys. Lett.* **65** (1994) 3344.
11. J. C. STURM, P. V. SCHWARTZ, E. J. PRINZ and H. MANOHARAN, *J. Vac. Sci. Tech. B* **9** (1991) 2011.
12. J. C. STURM, A. ST. AMOUR, Y. LACROIX and M. L. W. THEWALT, *Appl. Phys. Lett.* **64** (1994) 2291.
13. Medici™ is a trademark of Technology Modeling Associates, Inc., Palo Alto, CA.
14. H. SCHLANGENOTTO, H. MAEDER and W. GERLACH, *Phys. Stat. Sol. A* **21** (1974) 357.
15. X. XIAO, C. W. LIU, J. C. STURM, L. C. LENCHYSHYN and M. L. W. THEWALT, *Appl. Phys. Lett.* **60** (1992) 1720.
16. E. COHEN, M.D. STURGE, M. A. OLMSTEAD and R. A. LOGAN, *Phys. Rev. B* **22** (1980) 771.
17. S. C. JAIN and D. J. ROULSTON, *Solid-State Electronics* **34** (1991) 453.